Antiferromagnetic Resonance and Terahertz Continuum in α-$RuCl_3$

A. Little,[1,2] Liang Wu,[1,2,3,*] P. Lampen-Kelley,[4,5] A. Banerjee,[6] S. Patankar,[1,2] D. Rees,[1,2] C. A. Bridges,[7] J.-Q. Yan,[8] D. Mandrus,[4,5] S. E. Nagler,[6,9] and J. Orenstein[1,2]

[1]*Department of Physics, University of California, Berkeley, California 94720, USA*
[2]*Materials Science Division, Lawrence Berkeley National Laboratory, Berkeley, California 94720, USA*
[3]*Department of Physics and Astronomy, University of Pennsylvania, Philadelphia, Pennsylvania 19104, USA*
[4]*Department of Materials Science and Engineering, University of Tennessee, Knoxville, Tennessee 37996, USA*
[5]*Materials Science and Technology Division, Oak Ridge National Laboratory, Oak Ridge, Tennessee 37831, USA*
[6]*Quantum Condensed Matter Division, Oak Ridge National Laboratory, Oak Ridge, Tennessee 37830, USA*
[7]*Chemical Sciences Division, Oak Ridge National Laboratory, Oak Ridge, Tennessee 37830, USA*
[8]*Material Sciences and Technology Division, Oak Ridge National Laboratory, Oak Ridge,Tennessee 37830, USA*
[9]*Bredesen Center, University of Tennessee, Knoxville, Tennessee 37966, USA*

(Received 24 April 2017; revised manuscript received 7 August 2017; published 28 November 2017)

We report measurements of optical absorption in the zigzag antiferromagnet α-$RuCl_3$ as a function of temperature T, magnetic field B, and photon energy $\hbar\omega$ in the range ~0.3–8.3 meV, using time-domain terahertz spectroscopy. Polarized measurements show that threefold rotational symmetry is broken in the honeycomb plane from 2 to 300 K. We find a sharp absorption peak at 2.56 meV upon cooling below the Néel temperature of 7 K at $B = 0$ that we identify as the magnetic-dipole excitation of a zero-wave-vector magnon, or antiferromagnetic resonance (AFMR). With the application of B, the AFMR broadens and shifts to a lower frequency as long-range magnetic order is lost in a manner consistent with transitioning to a spin-disordered phase. From a direct, internally calibrated measurement of the AFMR spectral weight, we place an upper bound on the contribution to the dc susceptibility from a magnetic excitation continuum.

DOI: 10.1103/PhysRevLett.119.227201

When exchange interactions between neighboring spins in a magnetic system are at odds, the resulting frustration can lead to a highly entangled form of matter with no ordered ground state. Such highly correlated, liquidlike states have come to be known as quantum spin liquids (QSLs) [1,2]. The QSL state is markedly featureless and difficult to experimentally detect—there being no local order parameter or phase transition. Nonetheless, QSL candidates are of great interest both theoretically and experimentally because they can host emergent fractionalized excitations—wherein the electron is divided into quasiparticles with fractional quantum numbers [3].

Lattices exhibiting geometric frustration, specifically those based on triangular arrangements of spins such as the kagome lattice [4], have long been at the center of QSL research. A significant step in the development of QSL theory was an alternative, exactly solvable route proposed by Kitaev [5,6]. The Kitaev spin liquid (KSL) model consists of spin-1/2 particles arranged on a hexagonal lattice with an Ising exchange interaction between nearest neighbors. Frustration results from rotation of the Ising axis from bond to bond, rather than the geometry of the lattice. In the exact solution of the KSL model the spin Hamiltonian is recast in terms of Majorana fermions propagating on the landscape of a static Z_2 gauge field [6]. Exact analytical results for dynamical spin correlations can be derived [7], leading to predictions for the signatures of Majorana quasiparticles in inelastic neutron [8–10], Raman [11], and resonant x-ray [12] scattering.

Coupled with theoretical progress, interest in the KSL model was greatly stimulated by the suggestion [13,14] that Kitaev interactions could arise in real materials, such as iridates and ruthenates [15–17], as a natural consequence of spin-orbit coupling. Although it was found that these materials order magnetically at low T [18–25], interest in these systems as proximate Kitaev spin liquids has developed, accelerated by the idea that emergent KSL quasiparticles may exist despite the presence of magnetic order. α-$RuCl_3$ has risen to prominence in this line of research because crystals suitable for inelastic neutron scattering (INS) have been grown, whereas INS is notoriously difficult in iridate compounds. INS performed on α-$RuCl_3$ indicates a continuum of excitations extending to 15 meV and centered at the zero in-plane wave vector, in addition to magnon peaks below the Néel temperature T_N [26,27]. This spectrum has been interpreted in terms of the $\mathbf{q} = \mathbf{0}$ dynamical susceptibility of KSLs, in which fractionalization into Majorana fermions and Z_2 vortices creates a continuum of spin fluctuations above a small gap [8–10]. Interpretations in terms of an incoherent multimagnon continuum have also been advanced [28]. The search for spin liquid states in α-$RuCl_3$ has been further stimulated by the observation that magnetic order is destroyed by in-plane magnetic fields that are weak compared to the leading order exchange interactions, suggesting the existence of one or more quantum critical points and a variety of exotic phases occupying the B-T phase space [29–34].

Thus far, the dynamical response in α-$RuCl_3$ has been probed exclusively by inelastic scattering [26,27,35–37]. In this work, we use time-domain terahertz spectroscopy (TDS) to probe excitations in α-$RuCl_3$ in the frequency range 0.08–2 THz (energy range 0.3–8.3 meV) and magnetic field range 0–7 T. TDS is complementary to INS in exploring magnetic excitations, as it focuses on the $\mathbf{q} = \mathbf{0}$ response function with higher spectral resolution and a precise, internally calibrated, determination of absolute spectral weight. By contrast, INS accesses a near zero in-plane wave vector $\mathbf{q}_{ab}$ by selecting nonzero out-of-plane momenta $\mathbf{q}_c$, introducing the broadening and distortion of line shapes from dispersion along the c direction. Furthermore, the INS studies of α-$RuCl_3$ at $\mathbf{q}_{ab} = \mathbf{0}$ published to date are limited to energies above ~2 meV by the elastic scattering background. The ability of TDS to trace the spectrum and spectral weight of the magnetic response function to lower energies at high resolution is critical for achieving a theoretical understanding the effective spin Hamiltonian of α-$RuCl_3$ and the nature of its phases in the B-T plane.

The crystals used in this study exhibit a single thermal phase transition to zigzag antiferromagnetic order at a T_N of ~7 K and have been shown to contain few stacking faults [27]. Samples of α-$RuCl_3$ with a typical area of ~0.8 cm^2 and a thickness of 1 mm were mounted over an aperture on a copper plate. We measured terahertz transmission at near normal incidence such that the probing fields lie in the ab (honeycomb) plane.

TDS is based on measuring the transmission coefficient $t(\omega)$ of picosecond timescale electromagnetic pulses. In the weak absorption limit appropriate to a large gap Mott insulator such as α-$RuCl_3$, $|t(\omega)| \cong [4n/(n+1)^2] \exp[-\alpha(\omega)d]$, where $\alpha(\omega)$ is the frequency dependent absorption coefficient, n is the index of refraction, and d is the sample thickness (see Sec. I of the Supplemental Material [38]).

Before considering the frequency dependence of the absorption, we show that TDS probes the point group symmetry of the unit cell of α-$RuCl_3$. In the presence of threefold rotational symmetry (C_3), $t(\omega)$ will be independent of the direction of the terahertz field in the ab plane. To test for C_3, we measured $t(\omega)$ as the sample was rotated between a pair of crossed linear polarizers. The inset to Fig. 1(a) shows a polar plot of the transmitted amplitude as a function of the sample angle at room temperature. The observed anisotropy demonstrates that C_3 is broken at 300 K. The fourfold pattern of the polar plot indicates optical birefringence, that is, the existence of a pair of orthogonal principal axes with distinct values of the index of refraction. Laue x-ray diffraction on the same crystal confirmed that these directions correspond to the a and b axes depicted in Fig. 1(b) (see Sec. II of the Supplemental Material [38]). The optical birefringence is likely related to an in-plane distortion of the Ru hexagons in which the length of the pair of opposing Ru-Ru links parallel to the b axis is greater than the other two by ~0.2% [49,50].

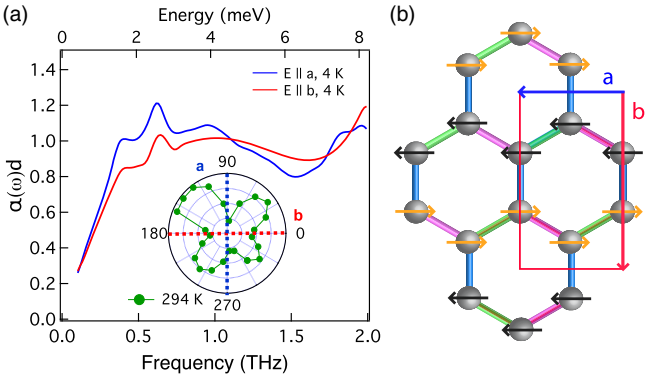

FIG. 1. (a) Optical density $\alpha(\omega)d$ with $\mathbf{E}$ parallel to axis $\mathbf{a}$ (blue) and axis $\mathbf{b}$ (red) at $T = 4$ K. Inset: polar plot of the transmitted terahertz electric field amplitude at 294 K as a function the rotation angle of a sample positioned between crossed polarizers. The principal axes are marked by dashed lines. (b) Zigzag antiferromagnetic order on the honeycomb lattice, with the $\mathbf{a}$ and $\mathbf{b}$ axis directions denoted by the blue and red arrows.

Although there are three equivalent orientations of this distortion, we note that the crystal under study must comprise largely a single such domain on the scale of the optical probe (~5 mm^2 area by 1 mm thickness) in order to show strong optical anisotropy.

In the main panel of Fig. 1(a), we plot the absorption $\alpha(\omega)d$ at 4 K with the $\mathbf{E}$ field polarized parallel to the $\mathbf{a}$ and $\mathbf{b}$ directions. A conspicuous feature of both spectra is the narrow peak at 0.62 THz (2.56 meV), which is superposed on a broad continuum of absorption with a low-energy cutoff. The spectra for the two orthogonal polarizations are distinctly different, showing that the breaking of C_3 observed at room temperature persists to low T. Thus, the phase transition at 150 K (which we observe optically, see Sec. III of the Supplemental Material [38]) must occur between crystal structures that each break C_3, for example, monoclinic → triclinic [51].

Figures 2(a) and 2(b) focus on the temperature dependence of the sharp peak in a zero magnetic field. The inset to Fig. 2(a) compares pulses transmitted through the sample at 2 and 15 K. In the main part of Fig. 2(a) we show, on an expanded vertical scale, the results of subtracting the terahertz transient measured at 15 K from those measured at various temperatures below the magnetic transition, for $\mathbf{B}(t) \perp \mathbf{a}$. The oscillations that grow with decreasing T are well described by damped sine waves $Ae^{-\Gamma t}\sin(\omega_R t)$, where A is the amplitude, ω_R is the resonant frequency, and Γ is the decay rate (see Sec. IV of the Supplemental Material [38]). Figure 2(b) illustrates the T dependence of A (left-hand scale) and Γ (right-hand scale).

As the 2.56 meV mode appears at T_N, it is natural to associate it with the resonant magnetic-dipole excitation of a $\mathbf{q} = \mathbf{0}$ magnon, which is known as antiferromagnetic resonance (AFMR) [39,52]. AFMR will appear at a nonzero frequency whenever $SU(2)$ spin rotation symmetry is broken by spin-orbit interactions, as are clearly present in

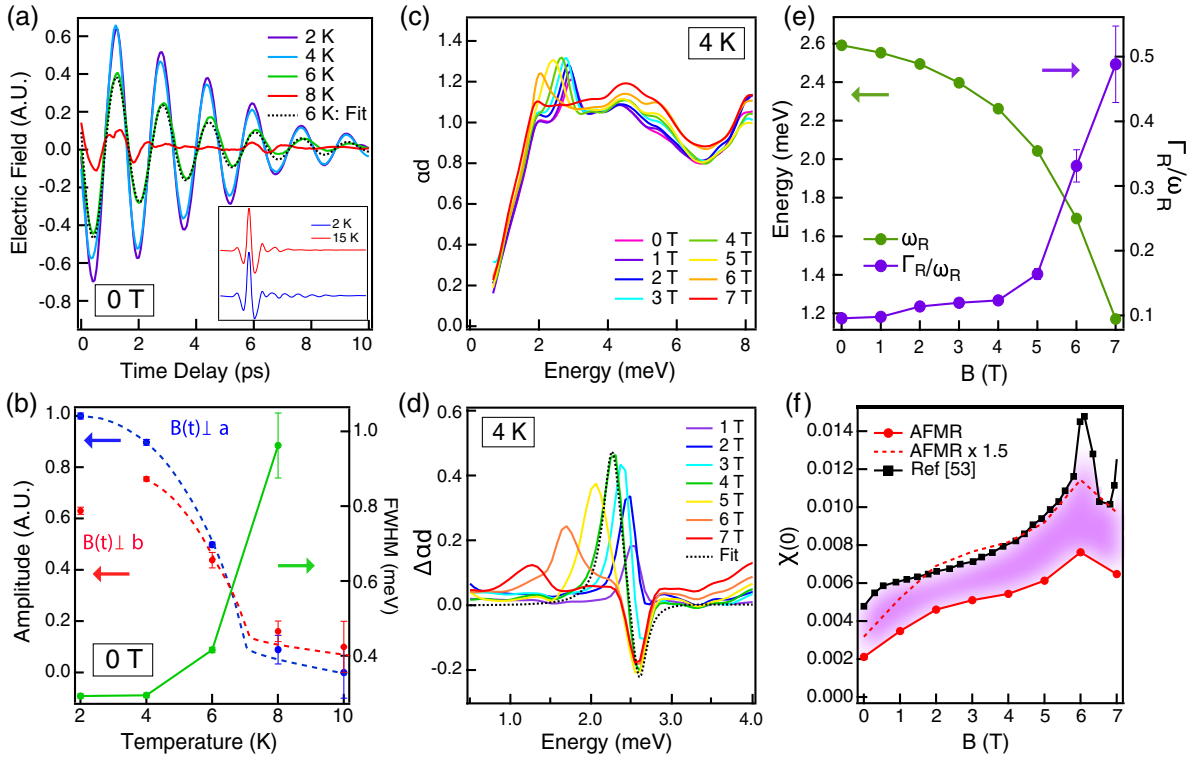

FIG. 2. (a) Coherent magnon emission measured in the time domain at 2, 4, 6, and 8 K on an expanded vertical scale. Inset: time trace of the transmitted terahertz **E** field at 2 K (blue) and 15 K (red). The 2 K pulse shows coherent magnon radiation while the 15 K pulse does not. (b) Resonance amplitude (left-hand scale) with $\mathbf{B}(t)\perp\mathbf{a}$ (blue) and $\mathbf{B}(t)\perp\mathbf{b}$ (red) and the FWHM along **a** (right-hand scale) as a function of temperature. The dashed lines are a guide to the eye. (c) The absorption spectrum at 4 K as a function of the magnetic field. (d) Absorption spectra with the dc B field parallel to the terahertz field $\mathbf{B}(t)$, both at 45° between the a and b axes. The zero-field spectrum is subtracted. (e) Dependence of the AFMR energy (left-hand axis) and inverse quality factor Γ_R/ω_R (right-hand axis) on the magnetic field. (f) The solid black and red circles show the static magnetic susceptibility $\chi(0)$ and the contribution to $\chi(0)$ from the $\mathbf{q}=\mathbf{0}$ spin wave, respectively, as a function of the magnetic field. The shaded region between indicates the maximum contribution from a magnetic excitation continuum.

α-$RuCl_3$. However, as translational symmetry is changed at T_N, it is also conceivable that the resonance results from folding to the zero wave vector of an acoustic phonon.

To test whether the resonance is indeed AFMR, we performed TDS as function of in-plane magnetic field from 0 to 7 T, obtaining the absorption spectra shown in Fig. 2(c). The resonant mode clearly shifts systematically to lower frequency with increasing B. As the periodicity of the antiferromagnetic order does not change with field [30], this observation demonstrates that the mode is not a zone-folded phonon and confirms its identity as AFMR.

Assuming that photons couple to the AFMR through the magnetic dipole interaction, we can evaluate the imaginary part of the dynamic magnetic susceptibility at zero wave vector, $\chi_2(\omega)$, associated with the peak. To focus on this component we subtract the zero-field spectrum from those measured with $\mathbf{B}\neq 0$; the resulting difference spectra are shown in Fig. 2(d). The strength of the absorption thereby is directly related to $\chi_2(\omega)$ via the relation

$$\alpha(\omega)d=\frac{\omega n d}{2c}\chi_2(\omega)=\frac{\omega T_{\mathrm{rt}}}{4}\chi_2(\omega). \tag{1}$$

Note that the absolute, as opposed to the relative, values of $\chi_2(\omega)$ are obtained directly from fundamental observables: the optical density αd and the pulse round-trip time T_{rt} (see Sec. I of the Supplemental Material [38]).

We find that for all values of the magnetic field the resonance can be well fit by a Lorentzian line shape, that is,

$$\chi_2(\omega,B)=\frac{S\omega\Gamma}{(\omega^2-\omega_R^2)^2+\omega^2\Gamma^2}, \tag{2}$$

where ω_R,Γ are now field dependent and $S(B)$ parametrizes the overall amplitude. The dashed line in Fig. 2(d) illustrates the quality of the fit for the 4 T difference spectrum (equally good fits for other fields are shown in Sec. IV of the Supplemental Material [38]). The variation with B of the resonant frequency and inverse quality factor Γ/ω_R obtained from the line shape analysis are shown in Fig. 2(e). The width of the resonance measured at a zero applied field, $\approx$300 μeV, is at least 5 times smaller than the $\mathbf{q}_{\mathbf{ab}}\approx\mathbf{0}$ peak observed by INS [27,53]. It is striking that although $\omega_R(B)$ decreases with increasing B, the resonance remains remains a well-defined, underdamped mode despite the loss of

long-range magnetic order that occurs at a critical field, $B_c \approx 7$ T. Recent experiments that extend electron spin resonance measurements to higher fields show that this mode persists through the transition spin-disordered state; its frequency reaches a minimum value of ≈1 meV at B_c [54] and thereafter increases linearly in proportion to $B - B_c$ [54,55].

A key issue in unravelling the physics of α-$RuCl_3$, in particular its proximity to a spin liquid ground state, is the existence and strength of a continuum of magnetic excitations at $\mathbf{q} = \mathbf{0}$ in addition to well-defined magnon modes. Terahertz spectroscopy directly addresses this issue by providing an autocalibrated measurement of $\chi_2(\omega)$ at zero wave vector. The thermodynamic sum rule, derived from the Kramers-Kronig relation, relates $\chi_2(\omega)$ to the dc magnetic susceptibility $\chi(0)$,

$$\chi(0) = \frac{2}{\pi}\int_0^\infty \frac{\chi_2(\omega')}{\omega'}\, d\omega'. \tag{3}$$

While Eq. (3) is valid in general, the contribution to the dc susceptibility of a mode described by the Lorentzian line shape of Eq. (2) is simply given by $\chi(0) = S/\omega_R^2$.

The thermodynamic sum rule allows us to place a bound on the strength of the $\mathbf{q} = \mathbf{0}$ magnetic continuum in α-$RuCl_3$. In Fig. 2(f) we compare the dc susceptibility associated with the spin wave resonance with recent measurements of $\chi(0, B)$ using low-frequency susceptometry [53]. Both the spin wave contribution and the total $\chi(0, B)$ grow with increasing field, maintaining a fixed proportionality for $B < 6$ T; this is highlighted by the dashed line, which shows $S(B)/\omega_R^2(B)$ scaled by a factor of 1.5. The shaded region between the two curves corresponds the dc susceptibility not accounted for by the AFMR. It is expected that in a quantum phase transition from a magnetically ordered phase to a QSL with fractional excitations, the spectral weight of spin wave modes would shift to a broadband magnetic continuum. Our spectra show instead that the contribution to the dc susceptibility from a magnetic continuum remains comparable in size to the contribution of the $q = 0$ spin wave, which remains a well-defined mode even approaching the critical magnetic field. This suggests that the $B_c \approx 7$ T transition cannot be straightforwardly interpreted as a transition to a QSL.

Finally, we discuss the broadband component of the terahertz absorption that is evident in Figs. 1(a) and 2(c). First, the thermodynamic sum rule argument described above rules out the possibility that the large observed continuum arises entirely from magnetic-dipole absorption. To show this, consider converting the entire $\alpha(\omega)$ to $\chi_2(\omega)$ using Eq. (1), and then integrating $\chi_2(\omega)/\omega$ with respect to ω to obtain a value for $\chi(0)$. As is already evident from comparison of the spectral weight of the resonant and broadband contributions to αd, the $\chi(0)$ that emerges from this calculation is far larger, by ≈30 times, than the measured value of 0.02 emu/mole (~0.005 in Systeme International units) [24]. We conclude that the dominant contribution to the broadband absorption must originate from electric, rather than magnetic-dipole coupling, as expressed, for example, in terms of an optical conductivity.

Figure 3 shows the optical conductivity $\sigma_1(\omega)$ at temperatures from 2 K to room temperature, converted from the absorption coefficient using the relation $\sigma_1(\omega) = 2nY_0\alpha(\omega)$, where $Y_0 = 377\ \Omega^{-1}$ is the admittance of free space (see Sec. I of the Supplemental Material [38]). A striking feature of the spectra is the lack of temperature dependence—in particular, the dropoff in $\sigma_1(\omega)$ below ≈1 meV remains well defined even at high temperatures where $k_BT \gg 1$ meV. The linear in ω cutoff below 1 meV evident in Figs. 1, 2(c), and 3 is a highly reproducible feature seen in all spectra. Further evidence for the decrease in $\sigma_1(\omega)$ below 1 meV is that the dc conductivity $\sigma(0)$ (shown as a solid red circle) is indistinguishable from the origin on the scale of Fig. 3 even at room temperature, where $\sigma(0) \sim 3 \times 10^{-4}\ \Omega^{-1}\,\mathrm{cm}^{-1}$.

At this point the origin of the broadband terahertz conductivity in α-$RuCl_3$ is not known, as the 0.3–8.3 meV energy scale is well below the range of expected optical transitions. Excitations across the Mott gap onset at 200 meV (~50 THz) [17] and the dominant dipole-active optic phonon resonance is found at ~35 meV (~8.5 THz) (see Sec. V of the Supplemental Material [38]). Lorentzian fits to this phonon mode yield a $\sigma_1(\omega)$ that is well below the measured value near 1 meV (see Sec. V of the Supplemental Material [38]). Although non-Lorentzian line shapes are found in many wide-gap insulators, the signatures of these acoustic-phonon assisted processes are strong temperature and featureless power-law frequency dependences, both of which are inconsistent with the spectra of Fig. 3.

Given the structure in the spectra on the meV energy scale, we believe it is possible that the terahertz absorption is related in some way to the spin degree of freedom. We note that

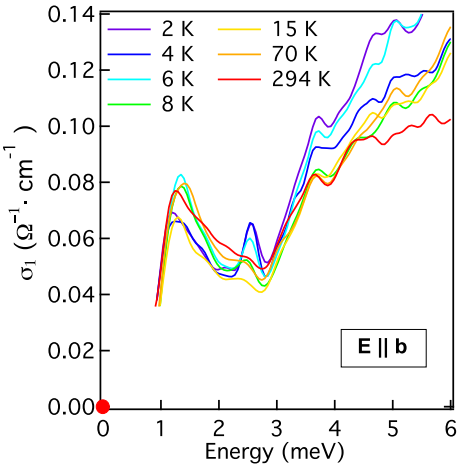

FIG. 3. Absorption spectra interpreted as optical conductivity, with **E** parallel to **b**.

features of the terahertz spectra, particularly the linear in ω low-energy cutoff shown in Figs. 1(a) and 2(c), closely resemble the dynamical spin structure factor predicted for the Kitaev-Heisenberg Hamiltonian [10]. Intrinsic mechanisms by which spin fluctuations in frustrated magnets acquire electric-dipole activity were described in Refs. [56,57]. The predicted optical conductance per atomic layer is either $\sim(e^2/h)(t/U)^3$ if the lattice is fixed, or $\sim(e^2/h)(t/U)^2$ if magnetoelastic coupling is considered (t and U are the hopping and Coulomb energies, respectively). Converting the spectra shown in Fig. 3 to conductance per Ru layer (see Sec. VI of the Supplemental Material [38]) yields an optical conductance of $\sim 10^{-4}(e^2/h)$ and of the same order as that found in the kagome compound Herbertsmithite [58].

To summarize, we measured the optical absorption of α-$RuCl_3$ at photon energies comparable to its magnetic exchange interactions, revealing a sharp magnon resonance and broadband optical conductivity that cuts off linearly below 1 meV. We tracked the evolution of the frequency, damping rate, and spectral weight of the dynamic susceptibility of the $\mathbf{q} = \mathbf{0}$ magnon as a function of the magnetic field. We believe this information is critical to understanding the role of the Kitaev and other, "parasitic," exchange interactions in determining the nature of the quantum critical points and novel phases of α-$RuCl_3$.

We thank N. P. Armitage, L. Balents, C. Batista, A. Potter, M. Serbyn, S. Winter, R. Valenti, and A. Vishwanath for helpful discussions, and H. Bechtel and M. Martin for support at the Advanced Light Source beam lines 1.4.3 and 1.4.4. Terahertz spectroscopy was performed at Lawrence Berkeley National Laboratory in the Spin Physics program supported by the Director, Office of Science, Office of Basic Energy Sciences, Materials Sciences and Engineering Division, of the U.S. Department of Energy under Contract No. DE-AC02-76SF00515. A. L. and L. W. were supported by the Gordon and Betty Moore Foundation's EPiQS Initiative through Grant No. GBMF4537 to J. O. at U.C. Berkeley. The work at ORNL was supported by the U.S. DOE, Office of Science, Basic Energy Sciences, Materials Sciences and Engineering Division, under Contract No. DE-AC05-00OR22725. A. B. and S. E. N. were supported by the U.S. DOE, Office of Science, Office of Basic Energy Sciences, Division of Scientific User Facilities. P. L.-K. and D. M. acknowledge support from the Gordon and Betty Moore Foundation's EPiQS Initiative through Grant No. GBMF4416.

A. L. and L. W. contributed equally to this work.

*liangwu@sas.upenn.edu

[1] L. Balents, Nature (London) **464**, 199 (2010).
[2] L. Savary and L. Balents, Rep. Prog. Phys. **80**, 016502 (2017).
[3] S. Sachdev, Nat. Phys. **4**, 173 (2008).
[4] T.-H. Han, J. S. Helton, S. Chu, D. G. Nocera, J. A. Rodriguez-Rivera, C. Broholm, and Y. S. Lee, Nature (London) **492**, 406 (2012).
[5] A. Y. Kitaev, Ann. Phys. (Amsterdam) **303**, 2 (2003).
[6] A. Kitaev, Ann. Phys. (Amsterdam) **321**, 2 (2006).
[7] G. Baskaran, S. Mandal, and R. Shankar, Phys. Rev. Lett. **98**, 247201 (2007).
[8] J. Knolle, D. L. Kovrizhin, J. T. Chalker, and R. Moessner, Phys. Rev. Lett. **112**, 207203 (2014).
[9] J. Knolle, D. L. Kovrizhin, J. T. Chalker, and R. Moessner, Phys. Rev. B **92**, 115127 (2015).
[10] X.-Y. Song, Y.-Z. You, and L. Balents, Phys. Rev. Lett. **117**, 037209 (2016).
[11] J. Knolle, G.-W. Chern, D. L. Kovrizhin, R. Moessner, and N. B. Perkins, Phys. Rev. Lett. **113**, 187201 (2014).
[12] G. B. Halász, N. B. Perkins, and J. van den Brink, Phys. Rev. Lett. **117**, 127203 (2016).
[13] G. Jackeli and G. Khaliullin, Phys. Rev. Lett. **102**, 017205 (2009).
[14] J. Chaloupka, G. Jackeli, and G. Khaliullin, Phys. Rev. Lett. **105**, 027204 (2010).
[15] S. Williams, R. Johnson, F. Freund, S. Choi, A. Jesche, I. Kimchi, S. Manni, A. Bombardi, P. Manuel, P. Gegenwart *et al.*, Phys. Rev. B **93**, 195158 (2016).
[16] K. A. Modic, T. E. Smidt, I. Kimchi, N. P. Breznay, A. Biffin, S. Choi, R. D. Johnson, R. Coldea, P. Watkins-Curry, G. T. McCandless *et al.*, Nat. Commun. **5**, 4203 (2014).
[17] K. W. Plumb, J. P. Clancy, L. J. Sandilands, V. V. Shankar, Y. F. Hu, K. S. Burch, H.-Y. Kee, and Y.-J. Kim, Phys. Rev. B **90**, 041112 (2014).
[18] X. Liu, T. Berlijn, W.-G. Yin, W. Ku, A. Tsvelik, Y.-J. Kim, H. Gretarsson, Y. Singh, P. Gegenwart, and J. P. Hill, Phys. Rev. B **83**, 220403 (2011).
[19] S. Choi, R. Coldea, A. Kolmogorov, T. Lancaster, I. Mazin, S. Blundell, P. Radaelli, Y. Singh, P. Gegenwart, K. Choi *et al.*, Phys. Rev. Lett. **108**, 127204 (2012).
[20] S. H. Chun, J.-W. Kim, J. Kim, H. Zheng, C. C. Stoumpos, C. Malliakas, J. Mitchell, K. Mehlawat, Y. Singh, Y. Choi *et al.*, Nat. Phys. **11**, 462 (2015).
[21] A. Biffin, R. D. Johnson, I. Kimchi, R. Morris, A. Bombardi, J. G. Analytis, A. Vishwanath, and R. Coldea, Phys. Rev. Lett. **113**, 197201 (2014).
[22] T. Takayama, A. Kato, R. Dinnebier, J. Nuss, H. Kono, L. S. I. Veiga, G. Fabbris, D. Haskel, and H. Takagi, Phys. Rev. Lett. **114**, 077202 (2015).
[23] H. S. Kim, V. Vijay Shankar, A. Catuneanu, and H.-Y. Kee, Phys. Rev. B **91**, 241110 (2015).
[24] J. A. Sears, M. Songvilay, K. W. Plumb, J. P. Clancy, Y. Qiu, Y. Zhao, D. Parshall, and Y.-J. Kim, Phys. Rev. B **91**, 144420 (2015).
[25] wH. B. Cao, A. Banerjee, J.-Q. Yan, C. A. Bridges, M. D. Lumsden, D. G. Mandrus, D. A. Tennant, B. C. Chakoumakos, and S. Nagler, Phys. Rev. B **93**, 134423 (2016).
[26] A. Banerjee, C. Bridges, J.-Q. Yan, A. Aczel, L. Li, M. Stone, G. Granroth, M. Lumsden, Y. Yiu, J. Knolle *et al.*, Nat. Mater. **15**, 733 (2016).
[27] A. Banerjee, J. Yan, J. Knolle, C. A. Bridges, M. B. Stone, M. D. Lumsden, D. G. Mandrus, D. A. Tennant, R. Moessner, and S. E. Nagler, Science **356**, 1055 (2017).

[28] S. M. Winter, K. Riedl, A. Honecker, and R. Valenti, Nat. Commun. **8**, 1152 (2017).
[29] R. Yadav, N. A. Bogdanov, V. M. Katukuri, S. Nishimoto, J. Van Den Brink, and L. Hozoi, Sci. Rep. **6**, 37925 (2016).
[30] J. A. Sears, Y. Zhao, Z. Xu, J. W. Lynn, and Y.-J. Kim, Phys. Rev. B **95**, 180411 (2017).
[31] S.-H. Baek, S.-H. Do, K.-Y. Choi, Y. Kwon, A. Wolter, S. Nishimoto, J. v. d. Brink, and B. Büchner, Phys. Rev. Lett. **119**, 037201 (2017).
[32] R. Hentrich, A. U. Wolter, X. Zotos, W. Brenig, D. Nowak, A. Isaeva, T. Doert, A. Banerjee, P. Lampen-Kelley, D. G. Mandrus *et al.*, arXiv:1703.08623.
[33] J. Zheng, K. Ran, T. Li, J. Wang, P. Wang, B. Liu, Z. Liu, B. Normand, J. Wen, and W. Yu, arXiv:1703.08474.
[34] I. A. Leahy, C. A. Pocs, P. E. Siegfried, D. Graf, S.-H. Do, K.-Y. Choi, B. Normand, and M. Lee, Phys. Rev. Lett. **118**, 187203 (2017).
[35] L. J. Sandilands, Y. Tian, K. W. Plumb, Y.-J. Kim, and K. S. Burch, Phys. Rev. Lett. **114**, 147201 (2015).
[36] K. Ran, J. Wang, W. Wang, Z.-Y. Dong, X. Ren, S. Bao, S. Li, Z. Ma, Y. Gan, Y. Zhang *et al.*, Phys. Rev. Lett. **118**, 107203 (2017).
[37] S.-H. Do, S.-Y. Park, J. Yoshitake, J. Nasu, Y. Motome, Y. S. Kwon, D. Adroja, D. Voneshen, K. Kim, T.-H. Jang *et al.*, arXiv:1703.01081.
[38] See Supplemental Material at http://link.aps.org/supplemental/10.1103/PhysRevLett.119.227201 for experimental methods, the determination of the index of refraction, and the crystallographic axes, and a discussion of FTIR spectra, AFMR, and optical conductivity, which includes Refs. [39–48].
[39] F. Keffer and C. Kittel, Phys. Rev. **85**, 329 (1952).
[40] G. Guizzetti, E. Reguzzoni, and I. Pollini, Phys. Lett. **70A**, 34 (1979).
[41] M. Sparks, D. F. King, and D. L. Mills, Phys. Rev. B **26**, 6987 (1982).
[42] E. Helgren, N. P. Armitage, and G. Grüner, Phys. Rev. B **69**, 014201 (2004).
[43] I. Jacobs, S. Roberts, and P. Lawrence, J. Appl. Phys. **36**, 1197 (1965).
[44] P. Ross, M. Schreier, J. Lotze, H. Huebl, R. Gross, and S. T. Goennenwein, J. Appl. Phys. **118**, 233907 (2015).
[45] J. Sheckelton, F. Foronda, L. Pan, C. Moir, R. McDonald, T. Lancaster, P. Baker, N. Armitage, T. Imai, S. Blundell *et al.*, Phys. Rev. B **89**, 064407 (2014).
[46] L. Pan, S. K. Kim, A. Ghosh, C. M. Morris, K. A. Ross, E. Kermarrec, B. D. Gaulin, S. Koohpayeh, O. Tchernyshyov, and N. Armitage, Nat. Commun. **5**, 4970 (2014).
[47] S. Zvyagin, D. Kamenskyi, M. Ozerov, J. Wosnitza, M. Ikeda, T. Fujita, M. Hagiwara, A. Smirnov, T. Soldatov, A. Y. Shapiro *et al.*, Phys. Rev. Lett. **112**, 077206 (2014).
[48] K. S. Novoselov, A. K. Geim, S. Morozov, D. Jiang, M. Katsnelson, I. Grigorieva, S. Dubonos, and A. Firsov, Nature (London) **438**, 197 (2005).
[49] R. Johnson, S. Williams, A. Haghighirad, J. Singleton, V. Zapf, P. Manuel, I. Mazin, Y. Li, H. Jeschke, R. Valentí *et al.*, Phys. Rev. B **92**, 235119 (2015).
[50] M. Ziatdinov, A. Banerjee, A. Maksov, T. Berlijn, W. Zhou, H. B. Cao, J. Q. Yan, C. A. Bridges, D. G. Mandrus, S. E. Nagler *et al.*, Nat. Commun. **7**, 13774 (2016).
[51] Note that the trigonal or rhombohedral structure has three-fold rotation symmetry along the stacking direction (c) of $RuCl_3$.
[52] T. Nagamiya, Prog. Theor. Phys. **6**, 342 (1951).
[53] A. Banerjee, P. Lampen-Kelley, J. Knolle, C. Balz, A. Aczel, B. Winn, Y. Liu, D. Pajerowski, J.-Q. Yan, C. Bridges *et al.*, arXiv:1706.07003 (2017).
[54] A. Ponomaryov, E. Schulze, J. Wosnitza, P. Lampen-Kelley, A. Banerjee, J.-Q. Yan, C. Bridges, D. Mandrus, S. Nagler, A. Kolezhuk *et al.*, arXiv:1706.07240 (2017).
[55] Z. Wang, S. Reschke, D. Hüvonen, S.-H. Do, K.-Y. Choi, M. Gensch, U. Nage, T. Rõõm, and A. Loidl, Phys. Rev. Lett. **119**, 227202 (2017).
[56] L. N. Bulaevskii, C. D. Batista, M. V. Mostovoy, and D. I. Khomskii, Phys. Rev. B **78**, 024402 (2008).
[57] A. C. Potter, T. Senthil, and P. A. Lee, Phys. Rev. B **87**, 245106 (2013).
[58] D. V. Pilon, C. H. Lui, T.-H. Han, D. Shrekenhamer, A. J. Frenzel, W. J. Padilla, Y. S. Lee, and N. Gedik, Phys. Rev. Lett. **111**, 127401 (2013).